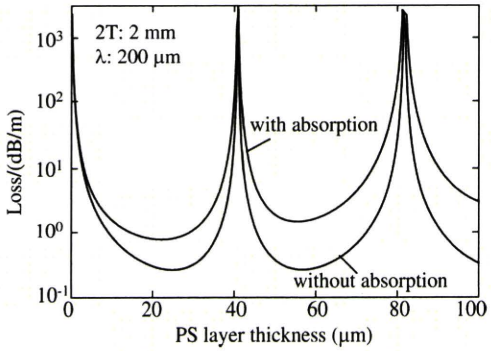

Fig. 1. Transmission loss of the HE_{11} mode as a function of PS layer thickness.

$356-j444$ [10] and $1.58-j3.58\times10^{-3}$ [11], respectively. It can be seen that the optimum PS layer thickness becomes smaller when dielectric absorption is taken into consideration. The optimum thickness for a nonabsorptive dielectric layer is 25 μm, and the loss is 0.26 dB/m. It is 22.3 μm for an absorptive PS layer, and the loss is 0.8 dB/m.

Figure 2 shows the transmission loss of the HE_{11} mode in the Au/PS-coated hollow fibers as a function of inner diameter. The PS layer is of optimized thickness as calculated in Fig. 1. The loss of the TE_{11} mode in the Au-coated hollow fiber is added for comparison. The additional loss introduced by dielectric absorption can be observed by comparing the two curves corresponding to Au/PS hollow fibers. The additional loss becomes larger for fibers with smaller inner diameters. When the inner diameter is smaller than 0.87 mm, the Au/PS hollow fiber has a higher transmission loss than the Au-coated hollow fiber. This means that the PS inner coating cannot reduce the loss. We also note that even for a nonabsorptive dielectric layer with $n_d=1.5$, it does not work for an Au-coated hollow fiber with a bore size smaller than 0.46 mm.

It has been reported that the optimum dielectric refractive index to minimize the loss of the HE_{11} mode is 1.41 when dielectric absorption is not considered [1]. Figure 3 shows the calculated transmission loss of the HE_{11} mode as a function of the dielectric refractive index. The optimum dielectric refractive index turns out to be greater than 1.41 for an absorptive dielectric layer. The optimum value is 2.1 in Fig. 3. For a refractive index smaller than 2.1, the loss increases rapidly. It indicates that dielectric materials of low refractive indices may not be suitable for inner coatings with the presence of dielectric absorption.

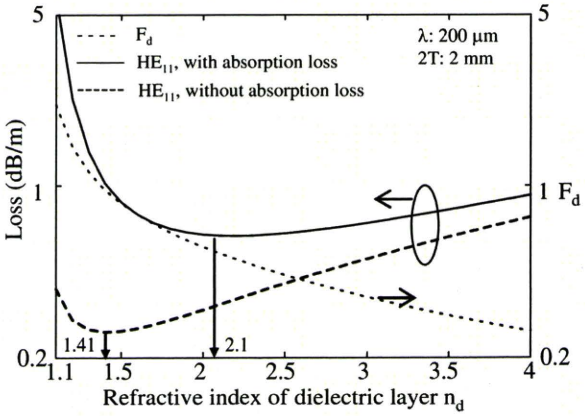

Fig. 3. Transmission loss of the HE_{11} mode as a function of n_d.

In Fig. 2 we have shown that the transmission loss of an Ag/PS hollow fiber may be higher than that of an Au-only hollow fiber owing to dielectric absorption. It is important to know the absorption tolerance (AT). We simply defined the AT as the absorption coefficient when the loss of a dielectric-coated metal hollow fiber is equal to that of a metal hollow fiber. Figure 4 shows the AT as a function of the refractive index of the dielectric layer. It is seen that the AT increases as the inner diameter becomes larger. The circle on each curve indicates the largest AT. The value of n_d, where the largest AT occurs, increases as the inner diameter becomes larger. It is interesting to find that the tolerance for the larger bore fiber is not as sensitive to n_d as is the small bore fiber. This can be seen from the shape of the curves. The tolerance for the 227 μm bore fiber decreases sharply when n_d changes, while the loss of the 500 μm bore fiber does not change so much when n_d changes. This also means that a big bore fiber has a large, useful n_d range.

Figure 5 shows ATs for the 200, 500, and 1000 μm bore hollow fibers. Absorption properties of four dielectric materials—polytetrafluoroethylene (PTFE),

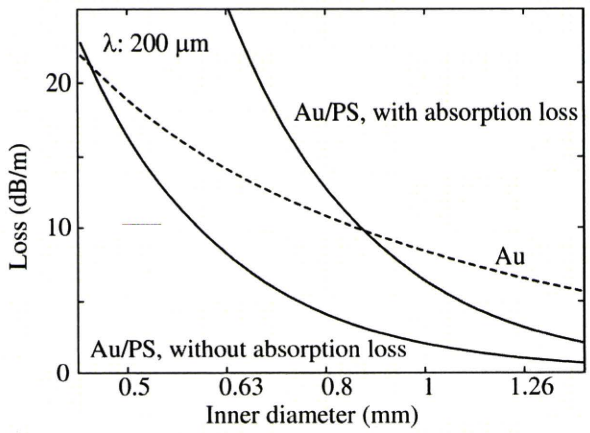

Fig. 2. Transmission loss of terahertz hollow fiber as a function of inner diameter.

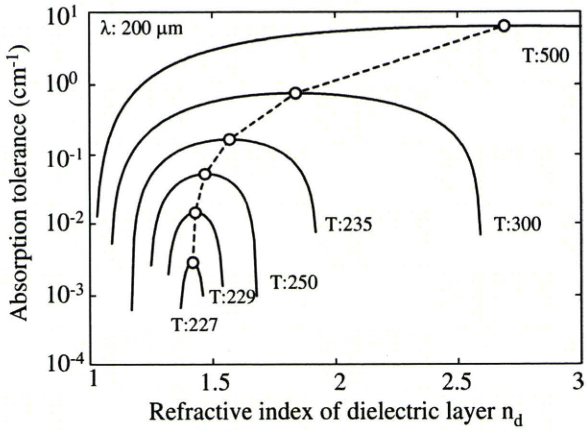

Fig. 4. AT as a function of dielectric refractive index.

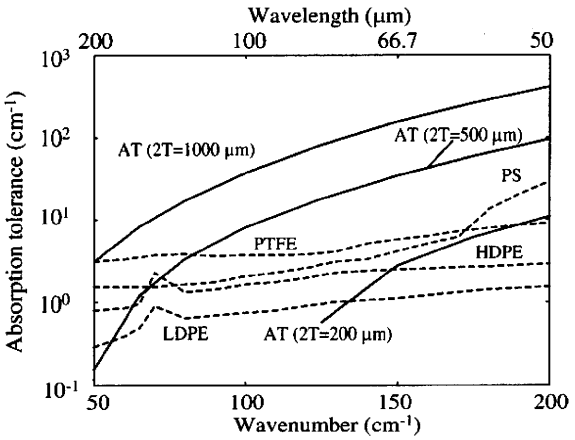

Fig. 5. AT and absorption spectra of polymers.

PS, high-density polyethylene (HDPE), and low-density polyethylene (LDPE) [11,12]—were added for comparison. n_d was 1.5 for the calculation, because the refractive indices of the four materials are all around 1.5 in the wavelength region from 50 to 200 μm. It can be observed that the tolerance decreases with the increase in the wavelength. From a wavelength of 50 to 200 μm, the AT decreases by more than 2 orders of magnitude. Take the 500 μm bore fiber, for example; all of the four materials are suitable as coating materials to reduce loss when the transmission wavelength is smaller 100 μm. However, none of these materials are usable when the wavelength is greater than 180 μm. For the 1000 μm bore fiber, all of the four materials are usable. On the other hand, when the bore diameter is 200 μm, the AT has no value in the wavelength region longer than 83 μm. It means that no dielectric material can reduce the loss in this case. As shown in Fig. 5, LDFE has low absorption in the terahertz region and can be one of the good choices as the dielectric materials.

In summary, the transmission characteristics of terahertz hollow fibers are more dependent on the dielectric absorption, because much thicker dielectric layers are required. With the presence of dielectric absorption, the optimum dielectric layer thickness becomes smaller, and the optimum dielectric refractive index becomes greater than 1.41. The transmission loss of a dielectric-coated metal hollow fiber can be greater than that of a metal hollow fiber owing to dielectric absorption. The AT decreases as the inner diameter becomes smaller or as the transmission wavelength becomes larger. In extreme cases of small diameter or large transmission wavelength, even a perfectly transparent dielectric layer cannot reduce the transmission loss of a metal-coated hollow fiber.

This research is supported by the Scientific Research Foundation for the Returned Overseas Chinese Scholars (33), the State Education Ministry, and the Shanghai Pujiang Program (7pj14012), as well as by the Ministry of Education, Science, Sports, and Culture of Japan (MESSC-JP) through a Grant-in-Aid for Scientific Research (B) (20360164) and (B) (19760240) 2008 and by the Health and Labor Science Research Grants (H20-nano-young-010) 2008.

References

1. M. Miyagi and S. Kawakàmi, J. Lightwave Technol. **LT-2**, 116 (1984).
2. J. A. Harrington, *Infrared Fibers and Their Applications* (SPIE, 2003).
3. I. Gannot, R. W. Waynant, A. Inberg, and N. Croitoru, Appl. Opt. **36**, 6289 (1997).
4. Y. W. Shi, K. Ito, L. Ma, T. Yoshida, Y. Matsuura, and M. Miyagi, Appl. Opt. **45**, 6736 (2006).
5. T. Ito, Y. Matsuura, M. Miyagi, H. Minamide, and H. Ito, J. Opt. Soc. Am. B **24**, 1230 (2007).
6. B. Bowden, J. A. Harrington, and O. Mitrofanov, Opt. Lett. **32**, 2945 (2007).
7. C. Themistos, B. M. A. Rahman, M. Rajarajan, K. T. V. Grattan, B. Bowden, and J. A. Harrington, J. Lightwave Technol. **25**, 2456 (2007).
8. M. Miyagi, A. Hongo, and S. Kawakami, IEEE J. Quantum Electron. **QE-19**, 136 (1983).
9. E. Snitzer, J. Opt. Soc. Am. **51**, 491 (1961).
10. E. D. Palik, *Handbook of Optical Constants of Solids* (Academic, 1998).
11. J. R. Birch, Infrared Phys. **33**, 33 (1992).
12. J. R. Birch, Infrared Phys. **30**, 195 (1990).

Laser brackets debonding - Tm:YAP, Nd:YAG, and GaAs diode lasers evaluation

Taťjana Dostálová[a*], Helena Jelínková[b], Jan Šulc[b]
Petr Koranda[b], Michal Němec[b], Ilja Ivanov[a], Mitsunobu Miyagi[c], Katsumasa Iwai[c]

[a] Charles University, 2nd Medical School
Department of Paediatric Stomatology, V úvalu 84, 150 06 Prague 5, Czech Republic
[b]Faculty of Nuclear Sciences and Physical Engineering
Czech Technical University, Břehová 7, 115 19 Prague 1, Czech Republic
[c]Sendai National College of Technology
4-16-1 Ayashi Chuo, Aoba-ku, Sendai, 989-3128, Japan

ABSTRACT

The study demonstrates the possibility of using laser radiation for ceramic bracket removing. Three laser radiations were examined for this effect, and the removing possibility and velocity together with enamel and pulp damage were investigated. The lasers used were: a diode-pumped Tm:YAP microchip laser, diode pumped Nd:YAG laser, and GaAs diode generating 1.9 μm, 1.44 μm, and 0.808 μm, respectively. The measurement of transmission and absorption of the basic element – bracket, adhesive resin, and enamel - was also made with the goal to explain the source of heat and bracket debonding. The explanation of the debonding effect is also presented.
From the results it is possible to conclude that the continuously running diode pumped microchip Tm:YAP laser having output power 1W can be a good candidate for the ceramic bracket debonding procedure.

Keywords: dentistry, orthodontics, ceramic bracket debonding, GaAs diode laser, Tm:YAP laser, Nd:YAG laser

1. INTRODUCTION

Esthetics is an important factor for patients seeking an orthodontic treatment. A perfect and healthy smile is also demanded by the modern society [1]. Many orthodontists are familiar with the term "laser". However, there is a lack of information regarding its application in the orthodontic practice [2, 3] where the laser can be used for gingivoplasty, gengivectomy, removal of gingival overgrowths, and frenectomies [4]. Recently, various laser techniques have been investigated also for brackets debonding. One of the possible used removal techniques is application of the heat generated by laser radiation on brackets. For this method, the CO_2, KrF, XeCl, Nd:YAG or Tm:YAP lasers were used [5, 6, 7, 8].
The aim of this study was, at first, to find a simple and reliable method which can ensure the laser radiation brackets removal without changes in the enamel structure. For that reason, a diode-pumped Tm:YAP microchip laser, diode pumped Nd:YAG laser, and GaAs diode generating 1.9 μm, 1.44 μm, and 0.808 μm, respectively, were used for removing ceramic brackets. During the debonding procedure, a very important thing is the quantitative control of the amount of thermal energy delivered to the ceramic bracket which may overheat the tooth [9]. Therefore, the second goal of this contribution was to measure the temperature increase by a thermocouple placed inside the tooth, and also by the thermo-camera images.

* E-mail: tatjana.dostalova@fnmotol.cz,Tel.+420 224433100,Fax: +420 224433102

Lasers in Dentistry XV, edited by Peter Rechmann, Daniel Fried, Proc. of SPIE Vol. 7162, 71620C

2. MATERIALS AND METHODS

2.1. Laser sources

As radiation sources, three laser systems were used: diode pumped Tm:YAP microchip laser generating wavelength of 1.9 μm, diode pumped Nd:YAG laser with 1.44 μm wavelength, and GaAs diode with 0.808 μm.

2.1.1. Diode GaAlAs laser

As near-infrared radiation source, a GaAlAs laser diode (LIMO HLU20F400) generating radiation at wavelength 808 nm was applied. The maximum output power 20W was obtained at the end of the fiber (core diameter 400 μm, numerical aperture 0.22). the generated radiation was unpolarized.

2.1.2. Diode pumped Tm:YAP laser

The second laser system was a longitudinally diode-pumped Tm:YAP laser operating at 1980 nm[9]. For pumping of this laser, a fiber-coupled diode LIMO HLU30F400-790 generating the 790 nm radiation was used. The maximum output power 3.8 W was measured behind the output coupler of the laser.

2.1.3. Nd:YAG laser

The third source was the diode-pumped Nd:YAG laser generating 1.444 μm radiation. The maximum output power obtained was 2 W. The laser was pumped by the diode LIMO HLU20F400 and special mirrors were used for the 1.444 μm resonator.

2.2. Tissue material

Ten human premolars of adolescent patients (age 11 to 15), extracted for orthodontic reasons, were used in the study. Ceramic brackets Facination 2 (Dentaurum, Germany) were bonded on these teeth, using the ConTec LC adhesive (Dentaurum, Germany). The enamel surface was cleaned with non-fluoride polishing paste, rinsed in a stream of water, and dried in a stream of oil-free air. An etching agent (ConTec Etch (Dentaurum, Germany)) was then applied for 15 seconds on labial enamel surface and rinsed in a stream of water for 10 seconds. After air-drying, the enamel showed a chalky white hue. On the prepared etched surfaces ConTec Primer was applied, slightly dispersed with air, and polymerized for 20 seconds using halogen lamp ELIPAR Free-Light 2 (3M ESPE, Germany). The ceramic brackets were coated with sufficient amount of ConTec LC adhesive, and each bracket was polymerized in frontal light stream with halogen lamp for 20 seconds (Figure 1 a).
To identify the temperature rise by a thermocouple, a hole was prepared inside the tooth opposite the bracket. All teeth with bonded brackets were placed in physiological solution and stored at 7°C.

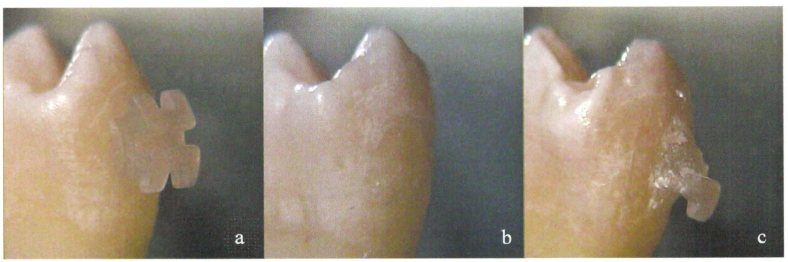

Figure 1. a- premolar with ceramic bracket; b- tooth surface after bracket removing; c – bracket crack.

2.3. Analyzing methods and measuring instruments

To characterize the laser radiation used, the mean power, the spectrum, the time development, and the spatial beam structure, the following instruments were used: Molectron energy/power meter EMP2000 with the PowerMax probe PM3 or PM10; Oriel monochromator model 77250 (50 μm wide slit); IR sensitive pyroelectric camera Pyrocam III, Spiricon (Figure 2); Tektronix oscilloscope TDS3052B (500 MHz, 5 GS/s) with InAs/InAsSbP photodiode (model PD36-05, IBSG Co, Ltd., spectral range 0.8-3.8 μm, rise time 150 ns).

All teeth with the brackets were photographed (before and after the treatment) by stereomicroscope Nikon SMZ-2T, Japan (Figure 1 a-c), connected with Mitsubishi CCD color video camera (CCD-100) and PC computer; temperature changes inside the tooth during the bracket irradiation were recorded by GMH 3210 digital thermometer; tooth surface temperature spatial distribution (progress and attenuation) was monitored by thermal imager-infrared camera Optilas – Electrophysics PV320L2E; the surface of the enamel after removing the bracket was analyzed by scanning electron microscope JSM 5510 LV Jeol, Japan. The teeth were processed in "low vacuum" (10 Pa) regime without desiccation. Back-scattered Electron Images were recorded using this technique (Figure 3, 4).

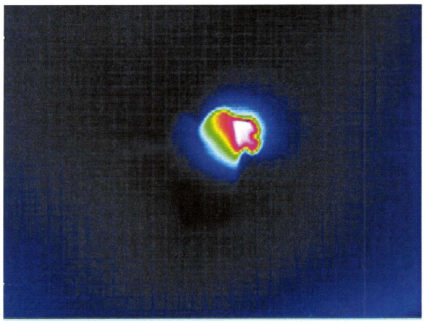

Figure 2. Result from IR sensitive pyroelectric camera Pyrocam III during temperature measurement of tooth 14.

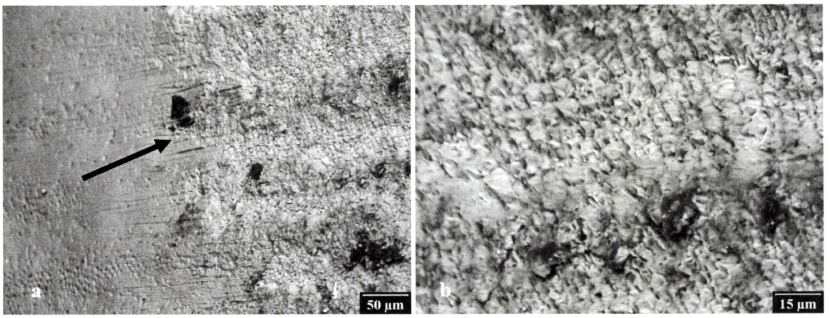

Figure 3. a - enamel surface after bracket debonding (arrow – bracket border); b – detail with open enamel prisms and rest of adhesive resin.

2.4. Experimental procedure

The output radiation from the particular laser was directed into the brackets. The power used in the particular irradiation was measured with power meter Molectron EPM 2000e connected with the probe PM3. The time of irradiation was 60 s and 90 s - with and without water cooling. The bracket with the tooth sample was heated by the laser light and after the chosen time interval the bracket was removed mechanically from the tooth surface. During the procedure, the temperature inside the tooth was recorded by NiCr-Ni thermocouple and GMH 3210 digital thermometer. Simultaneously, the tooth surface temperature spatial distribution was monitored by thermal imager PV320L2E.

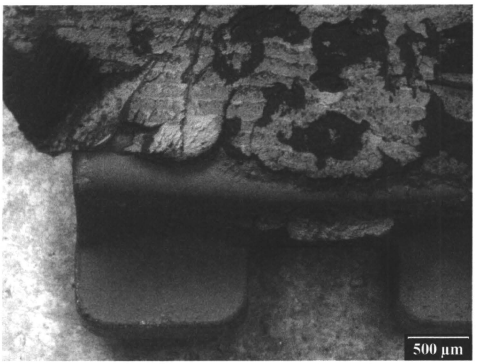

Figure 4. Ceramic bracket with the rest of ConTec LC adhesive in SEM.

3. RESULTS

3.1. Debonding procedure and temperature measurement

The irradiation conditions and results obtained are summarized in Figure 5. After the brackets were irradiated by the GaAs diode (0.808 µm), they could not be released even for 60 s irradiation. From the temperature profile measurement it is seen that the remaining radiation is transmitted through the tooth tissue and heats the thermocouple up to 14°C.
When Tm:YAP radiation was used, the heat was concentrated inside the bracket and adhesive resin, and after 60 s the bracket could be removed. With increasing the exposure time (up to 90 s) or radiation power (up to 2W), the debracketing speed was approximately the same. Differences were in the temperature inside the tooth. The optimum was found for the exposure time 60 s and water cooling application.
Similar results have been obtained for the Nd:YAG laser (1.444 µm), only the increase of temperature without and with cooling was steeper.

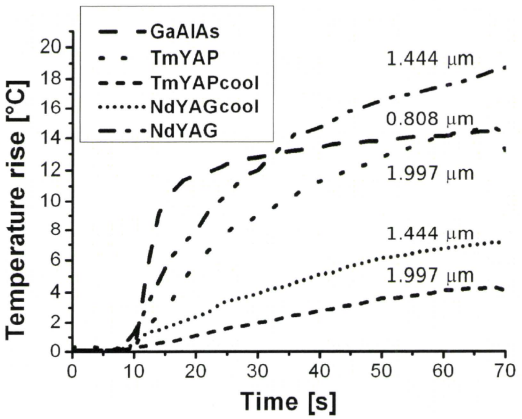

Figure 5. Time dependence of the temperature rise during irradiation by various types of radiations.

3.2. Photo and SEM investigation of the tooth after debonding

The GaAs diode 0.808 μm radiation is not effective for debonding (Figure 1 c). Therefore, for SEM measurements only the teeth treated by Tm:YAP (1.997 μm) and Nd:YAG (1.444 μm) were used (Figure 1a; 6 a). The results for both laser sources were similar and are seen in the Figures 6 (a-d). The ceramic bracket is directly connected with the enamel, an aesthetic quality is excellent (Figure 1 a; 6 a). After laser irradiation the bracket can be removed without cracks (Figure 1 b; 6 b). The rest of ConTec LC adhesive is visible on the enamel surface (Figure 1 b, 7 c). It is evident that after the bracket removal some changes did occur in the enamel surface in SEM (Figure 3 a, b; 6 d). The minimum damage was seen at 1 W and 60 s interval.

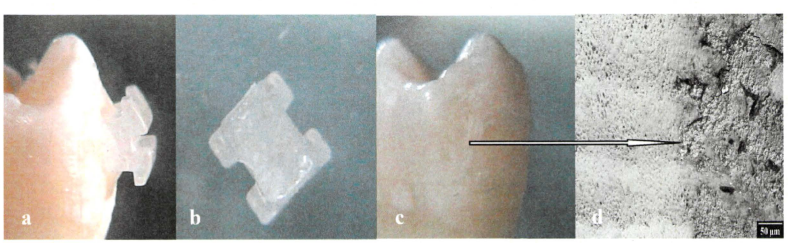

Figure 6. Photo and SEM evaluation: a - premolar with bracket; b – bracket after laser debonding; c – tooth after laser bracket debonding; d-SEM evaluation – detail from image c – magnification - unite segment 50 μm.

4. DISCUSSION

The principle of bracket debonding is to degrade the adhesive resin strength connecting the tooth and bracket. This can be done by laser radiation which can penetrate through the bracket to the adhesive resin and influence its strength bond to enamel. The results of our study generally agree with the previous studies, substantiating the fact that lasers can be used effectively to thermally soften the adhesive resin for removal of ceramic brackets [6, 7, 10]. From our investigation follows that it is possible to use laser radiation for easier bracket removal. The radiation applied must have the wavelength which has maximal absorption in the bracket and enamel by luting material formed connection, and minimal absorption in the tooth. If these criteria are fulfilled, radiation is an efficient helper in the debonding and no thermal damage [11] of the tooth appears after the procedure [10].
During the thermal debonding, a temperature gradient exists between the tooth surface and the pulp. The gradient of temperature rise from the tooth surface through the enamel and dentin does not follow a linear relationship during transient heating [9]. During laser irradiation, thermal ablation occurs and the bracket is removed from the enamel together with the rest of adhesive resin. From the scan investigation, it can be recognized that also part of the enamel can be sometimes partially removed with the bracket. Laser debonding is easier and little heat diffusion occurred.

5. CONCLUSION

The ceramic brackets debonding by the three various laser radiations were investigated. From the experiments performed it follows that continuously running lasers - the 1.997 μm Tm:YAP and 1.444 μm Nd:YAG with the power 1W acting for 60 s providing a reasonable dose for brackets tear off. From the SEM measurement results, minimum damage of enamel for this case was found.

ACKNOWLEDGEMENT

This research has been supported by the Grant of the Czech Ministry of Education No.MSM6840770022 "Laser systems, radiation, and modern optical applications".

REFERENCE

1. D. Sarver, "Principles of cosmetic dentistry in orthodontics: part 1. Shape and proportionality of anterior teeth", Am J Orthod Dentofac Orthop 126, pp. 749-753, 2004.
2. D. Sarver, M Yanosky,"Principles of cosmetic dentistry in orthodontics: part 2. Soft tissue laser technology and cosmetic gingival contouring. Am J Orthod Dentofac Orthop 127, pp. 85-90, 2005.
3. J. Tuner, L. Hode, Laser therapy: clinical practice and scientific background. Prima Books, Sweden, p 571, 2002
4. D. Sarver, M Yanosky,"Principles of cosmetic dentistry in orthodontics: part 3. Laser treatments for tooth eruption and soft tissue problems. Am J Orthod Dentofac Orthop 127, pp. 262-264, 2005.
5. N.R.Gorback, "Heat removal of ceramic brackets", J. Clin. Orthod.125, pp.42-47, 1991.
6. M.E. Vukovich, D.P. Wood, T.D. Daley, "Heat generated by grinding during removal of ceramic brackets", Am. J Orthod. Dentofac. Orthop. 9, p. 505- 512, 1990.
7. R.M.Tocchio, P.T.Williams, F.J.Mayor, K.G.Standing, " Laser debonding of ceramic orthodontic brackets", Am. J. Orthod. Dentofac. Orthop.,103, p. 155 - 163, 1993.
8. J.L. Rickabaugh, R.D.Marangoni, K.K. McCaffrey, "Ceramic debonding with the carbon dioxide laser.", Am. J. Orthod Dentofac Orthop.,110, 88-93, 1993.
9. H. Jelínková, J. Šulc, T.Dostálová, P. Koranda, M. Němec, "Bracket debonding by mid-infrared laser radiation" Laser Phys. Lett. 2009 in print
10. F.A. Rueggeberg, P. Lockwood, "Thermal debracketing of orthodontic resins" Am J Orthod Dentofac Orthop. 98, p. 56-65,1990.
11. L.Zach, G.Cohen, " Pulp response to externally applied heat", Oral Surg. Oral Med. Oral Pathol. 19, p. 515-530, 1965.

250 μm Inner Diameter Hollow Waveguide for Er:YAG Laser Radiation

Michal Němec[a*], Helena Jelínková[a]
Mitsunobu Miyagi[b], Katsumasa Iwai[b], Yuji Matsuura[c]
[a]Faculty of Nuclear Sciences and Physical Engineering
Czech Technical University in Prague, Břehová 7, 115 19 Prague 1, Czech Republic
[b]Sendai National College of Technology, Aoba-ku, Sendai 989-3128, Japan
[c]Graduate School of Engineering, Tohoku University, Sendai 980-8579, Japan

ABSTRACT

Advanced application of Er:YAG laser radiation in medical treatment requires a suitable, very precise delivery of this light to a target. In some cases (urology, cardiology, or endodontic treatments), thin waveguides are needed. Therefore a preliminary investigation was conducted with 250/360 μm inner/outer diameter hollow glass waveguides. The waveguide has inner coating made from cyclic olefin polymer and silver layers. All delivery systems were simple and consisted of lens, protector, and the waveguide. The laser source was the Er:YAG system working in a free-running regime and generating radiation at 2.94 μm wavelength. For testing, output laser energy up to 100 mJ with a repetition rate of 1 Hz was chosen. The output laser spatial profile was approximately TEM_{00} mode, so the structure changes behind the delivery system were readily detected. The energy delivery characteristics were also checked, and the transmission reached 77 %. The maximum input fluence into the waveguide was 200 mJ/cm^2, and no significant damages to waveguides were observed after the measurements.

Keywords: Hollow glass waveguide, Er:YAG laser, spatial structure.

1. INTRODUCTION

Delivery of radiation by a thin waveguide could be required in many applications. While optical fibers are utilized as standard systems in visible and near-infrared range of radiation, the transfer in mid-infrared radiation region requires a special delivery system, i.e. an articulated arm, special fiber up to 2.5 μm wavelength, and hollow waveguide. Selected hollow waveguides have several advantages. Due to air core, they have high power damage threshold, low insertion losses, and no end reflection. At present, the effort to obtain more effective delivery and minimize the dimension results in developing new waveguide types.[1-3] Also the beam spatial profile is an important parameter for applications, for example in ophthalmology, urology, dentistry, or micro-surgery.

This work is a continuation of on our long-time investigation of laser radiation delivery in a broad region (wavelengths from 750 nm to 2940 nm) by hollow waveguides with the inner diameter ranging from 250 μm to 1 mm[4, 5], in which the laser systems worked in free-running, Q-switching, or mode-locking regimes. The energy, temporal, and spatial characteristics were studied.

The goal of this work was to describe the delivery of Er:YAG mid-infrared laser radiation by 250/360 inner/outer diameter hollow glass waveguide with a length up to 100 cm.

2. MATERIALS AND METHODS

2.1. Er:YAG laser system

The Er:YAG laser radiation operating at wavelength 2.94 μm was generated in the free running long-pulse regime. As a laser active medium, a 100 mm long Er:YAG rod 5 mm in diameter was used and pumped by a xenon flash lamp. Both were placed into a LMI diffused ceramic pumping cavity (Marysol Technologies, Inc.). The 265 mm plan-parallel linear

* michal.nemec@fjfi.cvut.cz; phone +420 224 358 672; fax +420 222 512 735;

Optical Fibers and Sensors for Medical Diagnostics and Treatment Applications IX, edited by Israel Gannot,
Proc. of SPIE Vol. 7173, 71730H · © 2009 SPIE · CCC code: 1605-7422/09/$18 · doi: 10.1117/12.808097

resonator was formed by the total reflective copper mirror and by the dielectric flat output coupler with reflectivity 80 %.

The laser repetition rate was defined by the laser power supply and it ranged from 1 to 4 Hz. The maximum output energy and pulse length were 2.35 J and 550 μs, respectively[6]. In order to approximate a laser beam spatial structure to the fundamental TEM_{00} mode, a 3 mm aperture was inserted into the resonator[7]. Therefore, it was easy to recognize changes of profile behind the delivery system.

2.2. Delivery system

The delivery system is understood to be a coupling lens and waveguide. The coupling lens was selected according to the focusing beam spot diameter and inner waveguide diameter. In our case, we utilized a CaF_2 lens with 40 mm focal length.

The main part of the delivery system was a polymer coated silver hollow glass waveguides. From the surface to inside, its structure consisted of a polyimide protective layer, fused silica capillary, silver thin film, and dielectric polymer layer. As dielectric coating material, a cyclic olefin polymer (COP) was chosen because the layer from this material increases the reflectance of transmitted radiation on the inner surface of the waveguide. The thickness of the dielectric layer is dependent on wavelength of radiation. For the case of 2.94 μm it was 0.1 μm.

The primary parameters of the hollow waveguide are the inner and outer diameters, and we successfully produced 100/190, 250/360, 320/450, 540/700, 700/850 μm, or 1/1.5 mm with a possible length up to 2 m. The mechanical strength of the waveguides was determined by the silica glass tubing. The hollow glass COP waveguides also offer low-loss property, low aging effect, and, moreover, they are no toxic. Due to the absence of a bulk material in which the radiation is transmitted, the hollow waveguides have commonly lower losses, and in contrast to known silica fibers, special low-OH silica, or germanium fibers, they can also deliver high power radiation.

The inner diameter of the waveguide samples investigated was 250 μm and the outer diameter 360 μm. The different lengths of waveguides were 10 cm (Serial No. C25-3-0, C25-3-3), 100 cm (No.1, No.2), and 105 cm (No.3, and No.4); thanks to these diameters, very good flexibility of all waveguides was confirmed.

During adjustment stage, damages could arise on the waveguide input face and input inner layers; therefore a special tube-shaped protector for safekeeping was inserted behind the coupling lens. The waveguide was inserted into this protector.

2.3 Measuring instruments and methods

The basic parameters as radiation energy, pulse length, and spatial structure were followed. For the investigated delivery system, input and output characteristics are required. The laser energy was measured by two-channel Molectron ID 2000 Joulemeter/Ratiometer with probes - Molectron J25 and J25LP-Erbi (Coherent Inc.). The waveform for 3 μm range was investigated by infrared detector No.83614 connected to Tektronix 3052B scope (500MHz, 5 GS/s). The beam spatial profile was monitored by pyroelectric camera (Spiricon Pyrocam III, sensor dimension 12.4 x 12.4 mm) and computer.

Due to good stability of the generated radiation, the transmission characteristics were obtained from consecutive measurements of the input and output energy in front of and behind the delivery system. For each set of the pumping laser energy, the average of twenty values was measured.

3. RESULTS

3.1 Er:YAG laser radiation and coupling into waveguide

The Er:YAG laser was working with 1 Hz repetition rate. Due to 3 mm aperture in the resonator[7], the radiation was generated close to the fundamental TEM_{00} mode with $M^2 \cong 1$ (Fig.1).
For coupling, the CaF_2 lens with 40 mm focal length was used. The dependence of beam diameter on distance from focus plane is shown in Fig.2a (for 72 mJ laser energy). From the results in Fig.2b, 100 mJ maximum input energy was defined because appropriate beam diameter (~ 150 μm) for 250 μm waveguide is needed[8]. The measured beam diameter in focal

plane for the 86 mJ energy was 137 μm. The corresponding pulse length was 270 μs and input fluence 583 J/cm^2 (2.16 MW/cm^2).

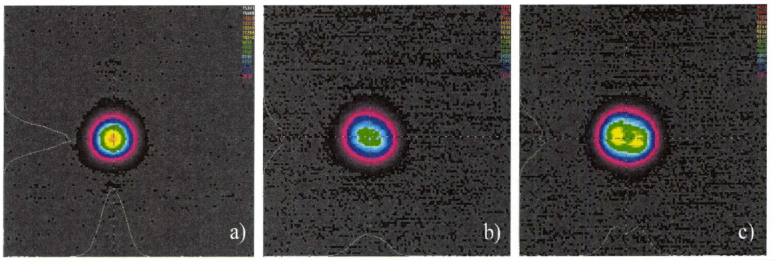

Fig. 1. Output beam spatial structure of 2.94 μm Er:YAG laser radiation a) 9 mJ b) 37 mJ c) 90 mJ (Spiricon Pyrocam III).

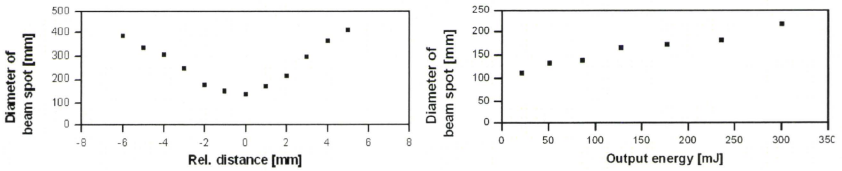

Fig. 2. Dependence of beam diameter on distance from focus plane for 72 mJ Er:YAG laser energy (a) and dependence of beam diameter in focal plane on output laser energy (b).

3.2 Delivery characteristics

The individual waveguides were inserted into protector and transmission characteristics were investigated. At first, 10 cm long waveguides were utilized. The dependence of output energy and transmission on input energy is seen in Fig.3. The recorded spatial structures are in Fig.4 and Fig.5. For both waveguide the transmission was approximately the same, i.e., T = 76 %. Waveguide No.1 was analogously investigated (Fig.6a, Fig.7). The transmission value was 61.3 %. Waveguide No.2 was initially 100 cm long, but it was cut into two 50 cm parts because the delivery was low both for guided He-Ne laser radiation and Er:YAG laser radiation (T ~ 26 %). Furthermore, one part showed low transmission (T ~ 23 %), but the second part reached up to 59 %. From this it follows that the first part of waveguide No.2 was damaged. The second part was measured in detail (Fig. 6 and Fig.8). Waveguide No.3 and No.4 were also investigated (Fig. 9, Fig 14, and Fig. 16).
The summary of energy delivery characteristics is shown in Table 1.

Table 1. Delivery characteristics of 2.94 μm Er:YAG laser radiation.

Serial No.	Length	Max. input energy	Max. output energy	Average transmission
C25-3-0	10 cm	89.9 mJ	67.7 mJ	76.5 %
C25-3-3	10 cm	90.3 mJ	66.6 mJ	76.1 %
No.1	100 cm	87.8 mJ	51.4 mJ	61.3 %
No.2	100 cm	40.8 mJ	10.6 mJ	26.0 %
No.2_part_A	50 cm	40.8 mJ	9.4 mJ	23.0 %
No.2_part_B	50 cm	93.2 mJ	53.4 mJ	59.1 %
No.3	105 cm	101.1 mJ	60.5 mJ	61.4 %
No.4	105 cm	103.6 mJ	64.8 mJ	64.7 %

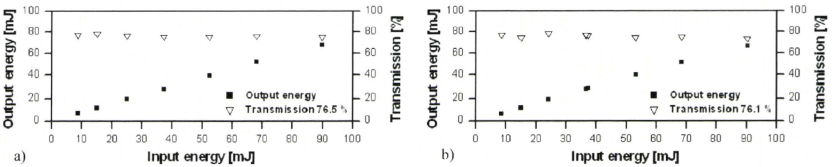

Fig. 3. Dependence of output energy and transmission on input energy for C25-3-0 (a) and C25-3-3 (b) waveguide with 250 μm inner diameter and 10 cm length. Average transmission was 76.5 % and 76.1 % for C25-3-0 and C25-3-3, respectively.

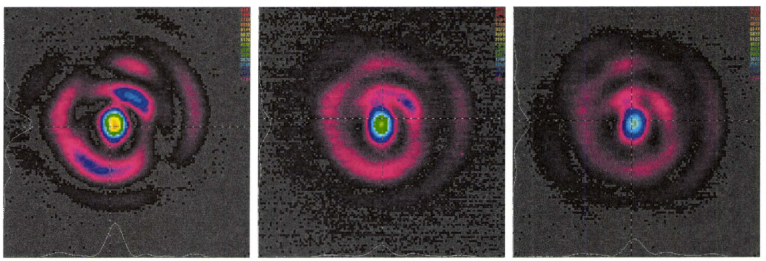

Fig. 4. Output beam spatial structure of 2.94 μm Er:YAG laser radiation behind C25-3-0 waveguide with 250 μm inner diameter and 10 cm length; a) 6.7 mJ b) 28.2 mJ c) 67.7 mJ (2D and 3D image, Spiricon camera).

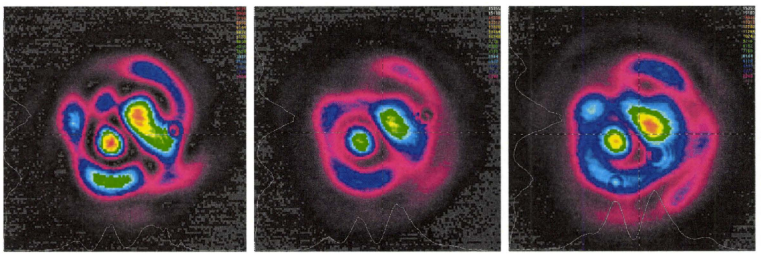

Fig. 5. Output beam spatial structure of 2.94 μm Er:YAG laser radiation behind C25-3-3 waveguide with 250 μm inner diameter and 10 cm length; a) 6.6 mJ b) 28.0 mJ c) 66.6 mJ (2D and 3D image, Spiricon camera).

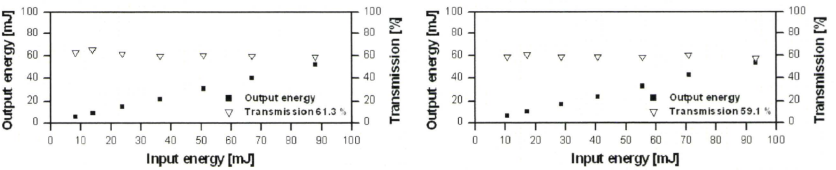

Fig. 6. Dependence of output energy and transmission on input energy for 100 cm waveguide No.1 (a) and 50 cm waveguide No.2_partB (b) with 250 μm inner diameter. Average transmission was 61.3 % and 59.1 % for No.1 and No.2_partB, resp.

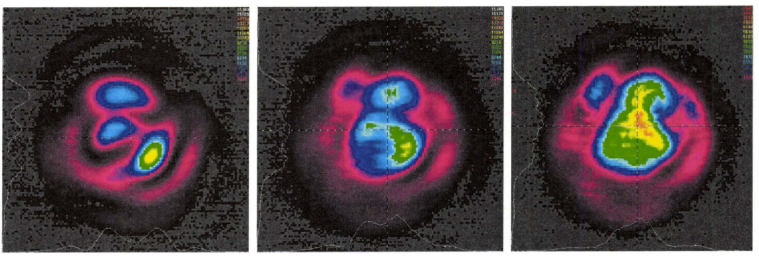

Fig. 7. Output beam spatial structure of 2.94 μm Er:YAG laser radiation behind waveguide No.1 with 250 μm inner diameter and 100 cm length; a) 5.3 mJ b) 21.8 mJ c) 51.7 mJ (2D and 3D image, Spiricon camera).

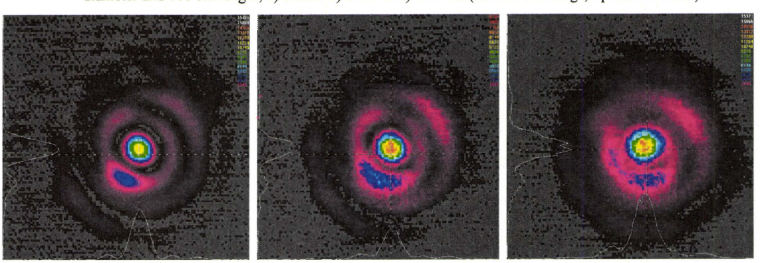

Fig. 8. Output beam spatial structure of 2.94 μm Er:YAG laser radiation behind waveguide No.2_part_B with 250 μm inner diameter and 50 cm length; a) 5.3 mJ b) 21.8 mJ c) 51.7 mJ (2D and 3D image, Spiricon camera).

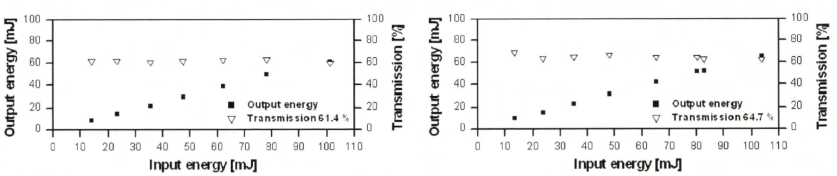

Fig. 9. Dependence of output energy and transmission on input energy for 105 cm waveguide No.3 (a) and 105 cm waveguide No.4 (b) with 250 μm inner diameter. Average transmission was 61.4 % and 64.7 % for No.3 and No.4, respectively.

Bending of waveguide

Before the transmission measurement of the bent waveguide, the 100 cm waveguide (No.1) was shorted to 98 cm because some damage was observed to its end and delivery decreased to 13 %. After cutting, the transmission was 56.7 % (Fig.10), approximately the same as for the first measurement (61.3 %, straight waveguide). Due to the similar transmission value, we could investigate the bending of this waveguide (angle 90°, R = 20 cm). The decrease in transmission value during bending was minimal, T ~ 54.6 % (Fig.10). The maximum input and output energies were 97 mJ and 52.4 mJ for straight and 98.9 mJ and 51.4 mJ for bent waveguide. The beam profiles behind the straight and bent waveguide are given in Fig.11 and Fig.12.

The results were also obtained for waveguide No.3 and No.4. The average transmissions were 61.4 % and 59.7 % for straight and bent waveguide No.3, respectively (Fig.13). Transmissions for waveguide No.4 were 64.7 % and 63.3 % (Fig.13). The output spatial structures are in Fig.14 (Fig.16) and Fig.15 (Fig.17) for straight and bent waveguide No.3 (No.4), respectively.

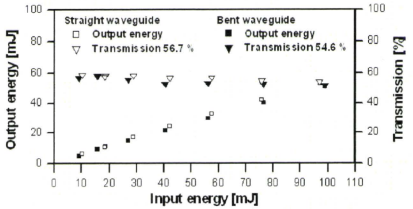

Fig. 10. Dependence of output energy and transmission on input energy for waveguide No.1 (98 cm) with 250 μm inner diameter for straight and bent waveguide. Average transmission was 56.7 % and 54.6 % for straight and bent waveguide, respectively.

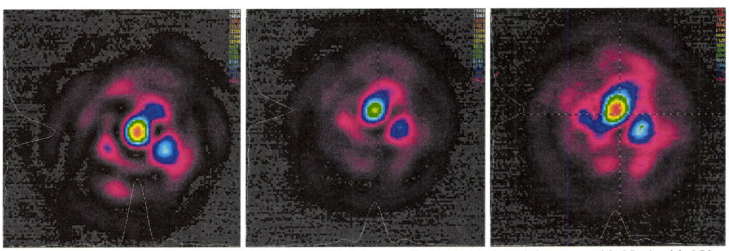

Fig. 11. Output beam spatial structure of 2.94 μm Er:YAG laser radiation behind straight waveguide No.1 with 250 μm inner diameter and 98 cm length; a) 6.0 mJ b) 23.8 mJ c) 52.4 mJ (2D and 3D image, Spiricon camera).

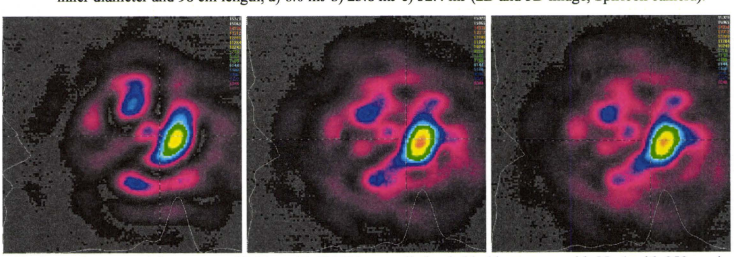

Fig. 12. Output beam spatial structure of 2.94 μm Er:YAG laser radiation behind bent waveguide No.1 with 250 μm inner diameter and 98 cm length; a) 5.2 mJ b) 21.4 mJ c) 51.4 mJ (2D and 3D image, Spiricon camera).

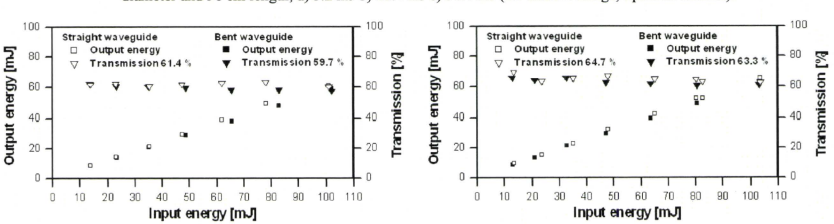

Fig. 13. Dependence of output energy and transmission on input energy for 105 cm long waveguide No.3 (a) and No.4 (b) with 250 μm inner diameter for straight and bent waveguide. Average transmission was 61.4 % and 59.7 % for straight and bent No.3 waveguide, respectively. For No.4 waveguide it was 64.7 % and 63.3 %.

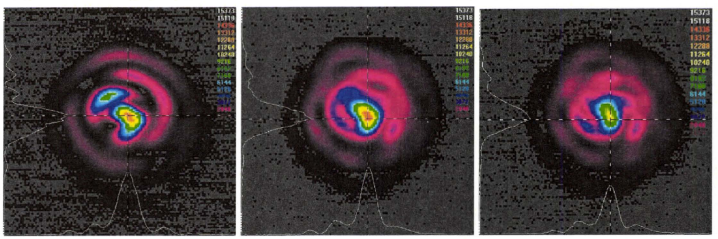

Fig. 14. Output beam spatial structure of 2.94 μm Er:YAG laser radiation behind straight waveguide No.3 with 250 μm inner diameter and 100 cm length; a) 8.6 mJ b) 29.1 mJ c) 60.5 mJ (2D and 3D image, Spiricon camera).

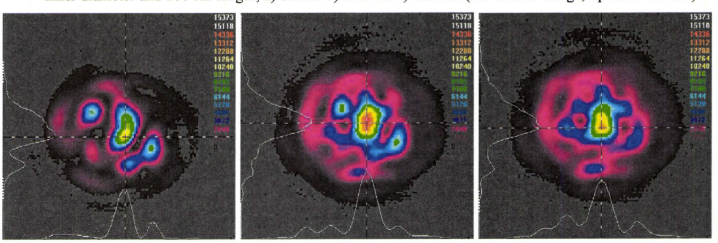

Fig. 15. Output beam spatial structure of 2.94 μm Er:YAG laser radiation behind bent waveguide No.3 with 250 μm inner diameter and 100 cm length; a) 8.5 mJ b) 29.0 mJ c) 58.9 mJ (2D and 3D image, Spiricon camera).

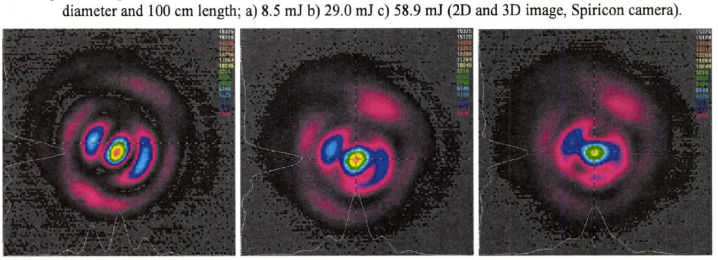

Fig. 16. Output beam spatial structure of 2.94 μm Er:YAG laser radiation behind straight waveguide No.4 with 250 μm inner diameter and 100 cm length; a) 9.3 mJ b) 31.8 mJ c) 64.8 mJ (2D and 3D image, Spiricon camera).

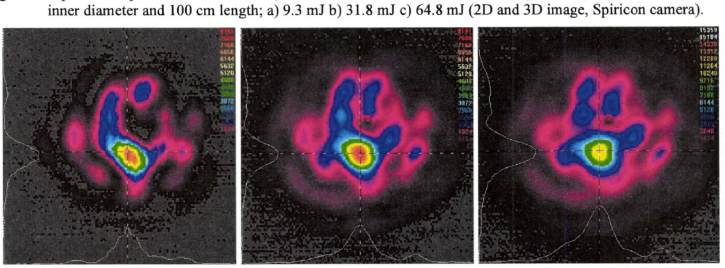

Fig. 17. Output beam spatial structure of 2.94 μm Er:YAG laser radiation behind bent waveguide No.4 with 250 μm inner diameter and 100 cm length; a) 8.5 mJ b) 29.5 mJ c) 63.1 mJ (2D and 3D image, Spiricon camera).

4. DISCUSSION AND CONCLUSION

In this work, the Er:YAG laser system was arranged and utilized. The laser worked in free-running regime at 2.94 μm wavelength and thanks to 3 mm aperture into resonator it generated approximately fundamental TEM_{00} mode. The maximum output energy used was 100 mJ.

As the principal aim of this work, the basic delivery characteristics of 250 μm inner diameter hollow glass waveguides for mid-infrared Er:YAG laser radiation were investigated. The waveguides were 10 cm, 50 cm, and 100 cm long. Besides energy transmissions, the modifications of the beam spatial profiles were recorded.

From the results for three ~ 100 cm long waveguides, it follows that transmission was exceeded 60 % (Table 1) for straight waveguides, and the decrease in delivery for 90° angle bending of waveguide was about 3 % (Table 2). As this value was reached for the adequately long waveguide, these waveguides can be sufficient for some applications where thin delivery systems are required (ophthalmology, cardiology, urology, and other microsurgery).

Table 2. Summary of energy delivery characteristics for straight and bent waveguides.

Serial No.	Length	Transmission for straight waveguide	Transmission for bent waveguide
No.1	98 cm	56.7 %	54.6 %
No.3	105 cm	61.4 %	59.7 %
No.4	105 cm	64.7 %	63.3 %

The delivered beam spatial structures for all investigated waveguides were modified in comparison with the input beam profile, but the changes are not significant. For all investigated straight and bent waveguides, the energy in the center has peak dominant value. So it means that the maximum delivered fluence occurred in a limited area, where we want to operate during the interaction with target.

It is possible to conclude that the 250 μm hollow glass waveguide delivery system can be used for transmitting the laser radiation to the target in specific medical and industrial applications.

ACKNOWLEDGEMENT

This research has been supported by the Center for Advanced Telecommunications Technology Research Foundations (SCAT) and by grant JSPS No. 17206033, as well as by the Grant of the Czech Ministry of Education No.MSM6840770022 "Laser systems, radiation and modern optical applications".

REFERENCES

[1] Nakazawa, M., Shi, Y., Iwai, K., Matsuura, Y., Zhu, X. and Miyagi, M., "Flexible hollow polycarbonate fiber for endoscopic infrared laser treatment," Proc. SPIE 6631, 66311A (2007).

[2] Dekel, B., Barkay Z. and Katzir, A., "The study of waveguides made by diffusion of Br into AgCl substrates and the transmission of mid-IR radiation through these waveguides," Optics Communications 199 (5-6), 383-388 (2001).

[3] Raif, J., Vardi M., Nahlieli, O. and Gannot, I. "An Er:YAG Laser Endoscopic Fiber Delivery System for Lithotripsy of Salivary Stones," Lasers Surg. Med. 38, 580-587 (2006).

[4] Jelínková, H., Němec, M., Šulc, J., Černý, P., Miyagi, M., Shi, Y.-W., and Matsuura, Y., "Hollow waveguide delivery systems for laser technological application," Progress in Quantum Electronics 28(3–4), 145–164 (2004).

[5] Němec, M., Jelínková, H., Sulc, J., Miyagi, M., Iwai, K., Shi, Y.-W. and Matsuura, Y., "Thin hollow glass waveguide for near IR radiation delivery", Proc. SPIE 6852, 68520W (2008).

[6] Němec, M., Jelínková, H., Šulc, J., Černý, P., Miyagi, M., Iwai, K., Abe, Y., Shi, Y. and Matsuura, Y., "Delivery of High Energy Radiation in Mid-infrared Spectral Region by Hollow Waveguides", Proc. SPIE 4957, 178-182 (2003).

[7] Němec, M., Jelínková, H., Fibrich, M., Koranda, P., Miyagi, M., Iwai, K., Shi, Y.W. and Matsuura, Y., "Mid-infrared radiation spatial profile delivered by COP/Ag hollow glass waveguide," Laser Phys. Lett.4(10), 761–767 (2007).

[8] Harrington, J.A., "Infrared Fibers and Their Applications", SPIE Press (2004).

The effect of dielectric absorption on the transmission characteristics of terahertz hollow fibers

Xiao-Li TANG[1], Yi-Wei SHI[1], Yuji MATSUURA[2], Katsumasa Iwai[3], Mitsunobu MIYAGI[3, 4]

1. Department of Communication Science and Engineering, Fudan University, Shanghai 200433, China. Email: ywshi@fudan.edu.cn

2. Graduate School of Engineering, Tohoku University, Sendai 980-8579, Japan

3. Sendai National College of Technology, Sendai, 989-3128, Japan

4. Miyagi National College of Technology, Sendai, 981-1239, Japan

Abstract

Hollow fiber with internal metal and dielectric coating films is one of the promising media for THz transmission. Although the dielectric layer can effectively reduce the transmission loss, it brings additional loss due to its absorption. It has been shown in mid-infrared region that the optimum thickness of the dielectric layer becomes smaller due to absorption. For terahertz hollow fibers, the film thickness of the dielectric layer become much larger and the transmission characteristics are more dependent on the dielectric absorption. The influences of dielectric absorption on the structure parameters of the dielectric-coated metallic hollow fibers are discussed. Calculation results show that the optimum refractive index of the dielectric layer, which is 1.41 for perfect transparent dielectrics, turns out to be greater. The absorption tolerance is also investigated considering the factors of inner diameter, the refractive index, and the transmission wavelength. It is shown that absorption tolerance decreases when the inner diameter becomes smaller or when the transmission wavelength becomes larger. In extreme cases of small inner-diameter or large transmission wavelength, the absorption tolerance is not existent. Because the loss of the dielectric-coated metallic hollow fiber is larger than that of metallic hollow fiber even the dielectric layer has no absorption. The calculation results are helpful to the structure design and material selection in the fabrication of terahertz hollow fibers.

1. Introduction

With the development of generation and detection techniques for terahertz radiation, the application of terahertz radiation is expanding rapidly in recent years. A low-loss, flexible THz waveguide is essential in many terahertz wave applications. Fibers that work well in the near infrared region are of high loss in THz wave due to material absorption. Recently, various kinds of waveguides have been suggested for efficient terahertz wave transmission, including metal wires, hollow core metal waveguides, plastic ribbon waveguides, photonic crystal fibers, Braggy fibers and plastic sub-wavelength fibers[1-6]. Dielectric-coated metallic hollow fibers have engendered growing interest over the past few years for their potential of low loss and flexibility. A low loss of 0.95 dB/m at 119 μm (2.5THz) was obtained by a 2 mm bore, 90 cm long

Optical Fibers and Sensors for Medical Diagnostics and Treatment Applications IX, edited by Israel Gannot, Proc. of SPIE Vol. 7173, 71730N · © 2009 SPIE · CCC code: 1605-7422/09/$18 · doi: 10.1117/12.808356

Ag/Polystyrene (PS)-coated hollow glass waveguides [7]. In a dielectric-coated metallic hollow fiber, a dielectric layer which can enhance the reflection rate was deposited over the metal layer to reduce the transmission loss. It has been proved an effective approach to produce low-loss fibers in the IR region as well as in the THz region [8]. However, the dielectric layer also brings additional losses due to its material absorption. It was reported that lossy dielectrics can be used as coating materials [9] for fiber operating in the IR region. While in the THz region, the influence is much more significant due to thicker dielectric film.

In this paper, the influences of dielectric absorption on the structure parameters of the hollow fiber were discussed based on the transmission line model [9]. The transmission modes of dielectric-coated metallic hollow fibers and metallic hollow fibers were briefly introduced in Section 2. The calculation results were given in Section 3. Finally the main results obtained in the paper were summarized and discussed.

2. Transmission modes of THz hollow fibers

As mentioned above, the dielectric layer in a hollow fiber has both positive effect and negative effect on the transmission loss. The overall effect can be investigated by comparing the transmission loss of a dielectric-coated metallic hollow fiber with that of a metallic hollow fiber. In this paper, the transmission losses are taken as the losses of the dominant modes since dielectric-coated metallic hollow fibers and metallic hollow fibers tend to propagate near single-mode energy. The cross-sectional image of a terahertz hollow fiber is shown in Fig. 1(a) and its transmission line model is shown in Fig.1 (b). In Fig. 1, d is the thickness of the dielectric layer, T is the inner radius, Z_{TE} and Y_{TM} are the normalized surface impedance and normalized surface admittance, Z_C and Y_C are the normalized impedance and admittance of the dielectric layer, Z_L and Y_L are the normalized impedance and admittance of the metal layer and x is the transverse electric length of the medium. When d = 0, Fig. 1 corresponds to a metallic hollow fiber; when d > 0, it corresponds to a dielectric-coated metallic hollow fiber.

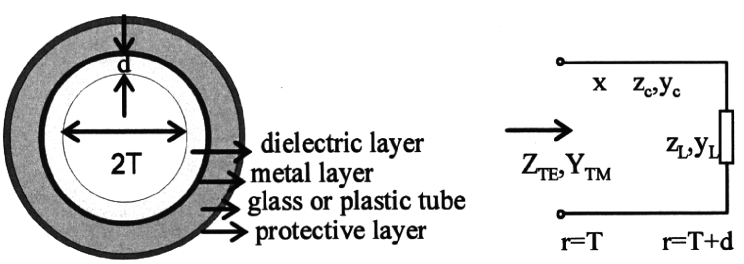

(a) (b)

Figure 1: Cross-section of THz hollow fiber and its transmission line model

In a metallic THz hollow fiber, TE_{11} mode has low theoretical losses. Furthermore, TE_{11} mode has high coupling efficiency to a linearly polarized Gaussian beam. The highest coupling efficiency is 90%. The experimental results showed that the measured losses of silver-coated THz hollow fibers are close to

the theoretical ones of the TE_{11} mode [2]. So the metallic THz hollow fibers mainly support TE_{11} mode with attenuation constant α_{TE11} [9]:

$$\alpha_{TE11} = \frac{k_0 \mu^2}{(k_0 T)^3} \frac{1}{1-\mu^{-2}} \mathrm{Re}\left(Z_L + \frac{(k_0 T)^2}{\mu^4 Y_L} \right), \quad (1)$$

Here, Re () denotes the real part of the numerical value in the bracket. k_0 is the wave number in vacuum and T is the inner radius. The phase constant μ is the first zero of the Bessel function $J_1(x)$, which is 1.841.

When a linearly polarized Gaussian beam is launched into a dielectric-coated metallic hollow fiber, mainly the HE_{1m} modes are excited. Among those modes, HE_{11} mode has the lowest loss and highest coupling efficiency. The highest coupling efficiency of HE_{11} mode to a linearly polarized Gaussian beam is 98.1% [11]. The experimental results showed that mainly the HE_{11} mode is transmitted when the structure parameters of the dielectric-coated metallic hollow fiber are optimized [7]. Without considering the dielectric absorption, the optimum dielectric layer thickness d_{opt} that minimizes the loss of HE_{11} mode is [9]:

$$d_{opt} = \frac{\lambda}{2\pi (n_d^2 - 1)^{1/2}} \left\{ \tan^{-1} \left[\frac{n_d}{(n_d^2 - 1)^{1/4}} \right] + s\pi \right\}, \quad s = 0, 1 \cdots, \quad (2)$$

Where λ is the wavelength, n_d is the refractive index of the dielectric layer. Equation (2) shows that d_{opt} can be infinite numbers of different numerical values. In practice, s = 0 is chosen for the consideration that the layer roughness increases with the layer thickness.

Applying the theory of transmission line model, one obtains the Z_{TE} and Y_{TM} in Fig.1 as:

$$Z_{TE} = z_C \frac{z_L + j z_C \tan(x)}{z_C + j z_L \tan(x)}, \quad (3)$$

$$Y_{TM} = y_C \frac{y_L + j y_C \tan(x)}{y_C + j y_L \tan(x)}, \quad (4)$$

For the dielectric-coated metallic hollow fiber with absorptive layer, the attenuation constant of the HE_{11} mode, denoted as α'_{HE11}, is

$$\alpha'_{HE11} = \frac{k_0 {\mu_0}^2}{2(k_0 T)^3} \mathrm{Re}(Z_{TE} + Y_{TM}), \quad (5)$$

Letting the complex refractive indices of the dielectric layer and the metal layer be n_d-jk_d and n-jk respectively, Equation (5) may be expressed as:

$$\alpha'_{HE11} = \alpha_{HE11} + \Delta\alpha, \quad (6)$$

Where α_{HE11} is the attenuation constant of the HE_{11} mode when dielectric absorption is not taken into consideration, $\Delta\alpha$ is the absorption loss introduced by dielectric layer.

$$\alpha_{HE11} = \frac{1}{2}\left(\frac{\mu_0}{2\pi}\right)^2 \frac{\lambda^2}{T^3}\frac{n}{n^2+k^2}\left(1+\frac{n_d^2}{(n_d^2-1)^{1/2}}\right)^2 , \tag{7}$$

$$\Delta\alpha = \alpha_{HE11} k_0 d \frac{1}{F_m} k_d F_d , \tag{8}$$

Where μ_0 is the first zero of the Bessel function $J_0(x)$, which is 2.405,

$$F_m = \frac{n}{n^2+k^2} \quad \text{and} \quad F_d = \frac{\frac{n_d}{n_d^2-1}+\frac{n_d}{\sqrt{n_d^2-1}}}{1+\frac{n_d^2}{\sqrt{n_d^2-1}}}$$

It can be observed in Equation (8) that additional loss $\Delta\alpha$ caused by absorption is proportional to the dielectric layer thickness. This explains why dielectric absorption has significant influence on the THz hollow fibers.

In Equation (6), α_{HE11} is proportional to the parameter F_m as indicated in Equation (7), while $\Delta\alpha$ is irrelevant to the parameter F_m as indicated by the combination of Equation (7) and Equation (8). Thus, the smaller the parameter F_m, the smaller the loss α'_{HE11}.

Substituting Equation (7) and Equation (8) into Equation (6), one can see that α'_{HE11} is proportional to $1/T^3$. That is, the transmission losses reduce rapidly with the increase of the inner diameter.

3. Calculation results

Firstly, the influences of dielectric absorption on the optimum thickness of the dielectric layer are investigated. Here, a THz hollow fiber with inner Au and PS coatings is considered for the fact that in the THz region PS has low absorption and the refractive index of Au is close to that of Ag. Furthermore, Ag/PS-coated hollow glass fibers had been fabricated and proved to be effective in the transmission of THz radiation [7]. The loss of the HE_{11} mode in an Au/PS-coated hollow fiber with the variation of the PS layer thickness is presented in Fig.2. In the calculation, the bore diameter is 2 mm and the wavelength is 200 μm. The complex refractive index of PS is 1.58-j0.0036 [12]. The periodic variation of the losses with the increase of film thickness d is consistent with Equation (2). In practice, the smallest one is normally adopted. It can be seen that the optimum PS layer thickness becomes smaller when dielectric absorption is taken into consideration. In Fig.2, the optimum thickness for non-absorptive PS layer is 25 μm with the lowest loss 0.26 dB/m. While for an absorptive PS layer it is 22.3 μm with the lowest loss 0.8 dB/m. The dotted line in Fig.2 indicates that the loss valley remains constant in the case of non-absorptive PS layer and increases with the PS layer thickness in the case of absorptive layer.

Next, transmission loss as the function of inner diameter was calculated. Figure 3 shows the calculation results for three cases, Au-coated hollow fibers, Au/PS-coated hollow fibers with dielectric absorption and